Available online at www.sciencedirect.com

ScienceDirect

journal homepage: www.elsevier.com/locate/he

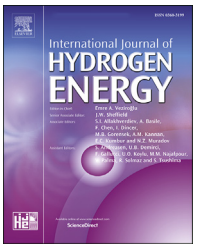

Roughness effects of gas diffusion layers on droplet dynamics in PEMFC flow channels

*Yanyao Bao, Yixiang Gan**

School of Civil Engineering, The University of Sydney, NSW, 2006, Australia

HIGHLIGHTS

- Numerical modelling was performed for droplets in flow channels of fuel cells.
- The importance of GDL roughness on effective water management is demonstrated.
- Modes of droplet movement are identified based on detachment ratio and location.
- Increasing RMS roughness can significantly improve water drainage efficiency.

ARTICLE INFO

Article history:
Received 25 February 2020
Received in revised form
10 April 2020
Accepted 26 April 2020
Available online 21 May 2020

Keywords:
Gas diffusion layer
Liquid removal
Surface roughness
PEMFC
Water transport

ABSTRACT

Water management remains one of the major challenges in optimising the performance of PEMFCs, in which liquid accumulation and removal in gas diffusion layers (GDLs) and flow channels should be addressed. Here, effects of GDL surface roughness on the water droplet removal inside a PEMFC flow channel have been investigated using the Volume of Fluid method. Rough surfaces are generated according to realistic GDL properties by incorporating RMS roughness and roughness wavelength as the main characteristic parameters. Droplet dynamics including emergence, growth, detachment, and removal in flow channels with various airflow rates are simulated on rough substrates. The influences of airflow rate on droplet dynamics are also discussed by comparing the detachment time and droplet morphology. The liquid removal efficiency subject to different surface roughness parameters is evaluated by droplet detachment time and elongation, and regimes of detachment modes are identified based on the droplet breakup location and detachment ratio. The results suggest that rough surfaces with higher RMS roughness can facilitate the removal of liquid inside flow channel. Whilst surface roughness wavelength is found less significant to the liquid removal efficiency. The results here provide qualitative assessments on identifying the key surface characteristics controlling droplet motion in PEMFC channels.

Introduction

The increasing energy consumption, existing nature of traditional energy sources, and raising awareness for climate change alleviation have propelled researchers to investigate renewable and sustainable energy as alternatives. Among various newly proposed renewable energy devices like wind turbines [1], photovoltaic panels [2], solar thermal systems [3]

* Corresponding author
E-mail address: yixiang.gan@sydney.edu.au (Y. Gan).
https://doi.org/10.1016/j.ijhydene.2020.04.228

and so on, hydrogen fuel cells have become an ideal candidate as energy-conversion devices for generating portable, automotive, and distributed power applications [4,5]. One of the most widely used fuel cell types is polymer electrolyte membrane fuel cells (PEMFCs) as they have advantages including relatively low operation temperature (60–90°C), quick start-up procedure, and simpler design [6,7]. Nevertheless, liquid water removal from PEMFCs should be carefully monitored because water management plays an important role in maintaining the optimal performance and durability of PEMFCs [8,9]. Whilst the membrane needs to be sufficiently hydrated to ensure the practical ionic conductivity, excessive liquid water accumulated in the gas diffusion layer (GDL) and flow channels could block the pathways for reactants thus resulting in performance degradation of PEMFCs. Liquid accumulation and transport in the PEMFC components have been extensively investigated to facilitate proper water management [10–12].

Understanding the liquid dynamics inside the flow channel greatly benefits the water management of PEMFCs, and several strategies have been proposed to overcome the operational deficiency caused by excessive water in diffusion media and flow channels. Firstly, water removal efficiency is significantly influenced by the material properties of GDL, which is typically made by carbon fibre or carbon cloth with high porosity and electrical conductivity [13,14]. PTFE (polytetrafluoroethylene) or FEP (fluorinated ethylene propylene) is usually applied on GDL to increase the hydrophobicity of the material, and therefore to assist the water drainage process during the operation of PEMFCs. Studies have shown that the wettability condition of GDL has significant influences on droplet detachment size [15] and water drainage efficiency [16]. Applying PTFE coating can improve the hydrophobicity of GDL material, and the liquid removal efficiency is enhanced by increasing PTFE loading where the droplets are found to detach with smaller diameters. Some researchers have managed to manipulate the spatial distribution of wettability in GDL to facilitate the liquid removal and reactant delivery in PEMFCs [17,18]. In addition to the wettability of GDL material, the operational conditions of PEMFCs also strongly affect the water accumulation and distribution, in which the airflow rate [19–21], operation temperature [22,23], operating pressure [24] and reactants humidity [25] are investigated. Finally, various geometrical configurations of the flow fields have been proposed by researchers to mitigate the water accumulation, including pin-type [26,27], parallel/straight [28,29], serpentine [30,31], integrated [32], interdigitated [33], and so on.

However, to the best of authors' knowledge, only few studies have been conducted to investigate the effects of GDL surface roughness on the efficiency of water removal inside PEMFCs [34–38]. The heterogeneity of GDL material is revealed by SEM images as shown in Fig. 1. The complex and nonuniform structures of GDL serve as the bottom substrate of flow channel, and the rough surface can significantly influence the liquid water transport and distribution in PEMFCs. Some researchers reconstructed GDL surface structures with patterned elements to represent the actual roughness, and they investigated the effects of surface roughness on water removal in PEMFC flow channel based on numerical models [34–37]. For example, He et al. [34] generated the rough surfaces by rectangle and triangle elements, and the roughness is defined as the ratio between the unit element and channel height. The results highlighted that increasing roughness element height facilitates the water drainage on hydrophilic surface, and the triangle elements perform better than rectangle elements in terms of water removal efficiency. Chen et al. [36] generated rough GDL surface by arrays of cubic columns, and roughness is characterised by column size and spacing. An analytical model is developed to predict the detachment of emerging droplets based on the balance between detaching and retention forces. The results underlined that the droplet removal time and coverage ratio decrease with the increase of surface roughness. Chen et al. [37] further examined the droplet transport inside flow channel with different layouts of GDL carbon fibre such as crisscross distributions, parallel distributions, directional distributions, and orthogonal distributions. It turned out that the surface microstructures influence the liquid water removal, and the directional distributions of carbon fibres best facilitate the liquid transport and reduce flooding. Ding et al. [35] investigated the formation and growth of liquid emerging from inlet pores of GDL with different number and diameter of inlet pores are simulated, and found the surface microstructures assist the liquid removal process especially for highly hydrophilic or hydrophobic cases. In addition, Ashrafi and Shams [38] modelled 2D rough surfaces characterised by different RMS roughness $(R_q)$and roughness density (R_d) values, showing that increasing R_q and R_d lead to the increase of pressure drop, droplet elongation and water retention, but decrease the amount of water adhered to the top wall.

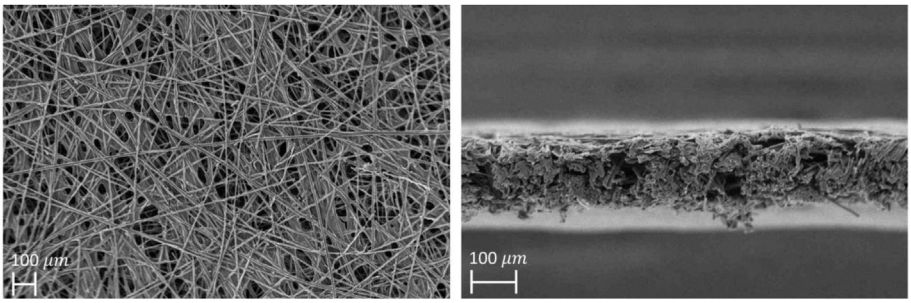

Fig. 1 – GDL fibre surface (left) and side view (right) by SEM scanning.

Nevertheless, the above-mentioned studies either simplified the surface roughness of GDL material by modelling patterned elements which leads to insufficient representation of surface roughness, or the dynamic processes of droplet emerging from the GDL layer to flow channel are not fully incorporated. Experimental observations serve as powerful tools to reveal the droplet dynamics inside the PEMFCs [39–42]. However, there are certain limitations for both in-situ and ex-situ techniques due to the differences in time and length scales between experimental setup and realistic operation conditions. Therefore, the computational fluid dynamics (CFD) methods are applied to provide valuable solutions to the gas-liquid interaction problems in PEMFCs [36,38,43–45]. CFD models are capable of handling strong deformation of the droplet, as well as reproducing different flow regimes such as droplet flow, film flow, and slug flow. In this study, a 2D Volume of Fluid (VOF) model is applied to investigate the liquid removal efficiency on rough surfaces considering the droplet emergence, growth, detachment and removal. Rough surfaces characterised by RMS roughness (R_q) and roughness wavelength (R_w) are constructed to match realistic GDL material roughness properties. The effects of GDL surface roughness and airflow rate on liquid removal efficiency are examined by comparing droplet detachment time and elongation, and the different detachment regimes and flow patterns are identified according to droplet breakup location and detachment ratio.

Numerical model

In this section, we will introduce the 2-dimensional Volume of Fluid (VOF) method to study the gas-liquid interaction inside the flow channel of PEMFC. The flow channels are modelled with a rough GDL, with variable roughness features to perform sensitivity studies. It is noteworthy that 2D computational models were selected in this work to access meaningful statistical data for multiple cases over rough surfaces with random features. Thus, the overall computational cost with over 160 cases simulated were significantly reduced. Moreover, this study mainly focuses on the effects of surface roughness by comparing the relative differences of droplet dynamics among multiple 2D cases, where 2D results can be qualitatively compared with similar 3D numerical solutions as shown later in the result part.

Numerical method

In the VOF method, immiscible fluids are modelled by solving a single set of momentum equations shared by both phases, and the interface between phases is tracked in each computational cell throughout the domain. The volume fraction (C) of liquid phase ranges from 0 to 1, and it has a value of 1 when the cell is occupied by liquid and 0 is assigned for gas. The effective properties of fluid such as density and dynamic viscosity, are weighted average values in each cell based on the volume fraction equation:

$$\rho = \rho_l C + \rho_g (1 - C), \tag{1}$$

$$\mu = \mu_l C + \mu_g (1 - C), \tag{2}$$

where ρ is density, μ is dynamic viscosity, and subscripts l and g represent liquid and gas phases, respectively. The continuity equation and the Navier–Stokes momentum equation are applied as governing equations to model all fluids in the computational domain:

$$\frac{\partial \rho}{\partial t} + \nabla \cdot (\rho \boldsymbol{v}) = 0, \tag{3}$$

$$\frac{\partial (\rho \boldsymbol{v})}{\partial t} + \nabla \cdot (\rho \boldsymbol{v}\boldsymbol{v}) = -\nabla p + \nabla \cdot \left(\mu \left(\nabla \boldsymbol{v} + \nabla \boldsymbol{v}^T\right)\right) + \rho g + \boldsymbol{F}_\gamma, \tag{4}$$

where $\boldsymbol{v}$ is the fluid velocity, p is the pressure, and $\boldsymbol{F}_\gamma$ is the surface tension force.

The surface tension force is modelled following the continuum surface force (CSF) model [46]:

$$\boldsymbol{F}_\gamma = 2\gamma \frac{2\rho k_l \nabla C}{(\rho_l + \rho_g)}, \tag{5}$$

where γ is the surface tension (unit: N/m), k_l is the surface curvature of the liquid droplet and it is computed from local gradients in the surface normal at the interface:

$$k_l = \nabla \cdot \boldsymbol{n}_l, \tag{6}$$

where $\boldsymbol{n}_l$ is the unit interface normal, and it can be approximated from the local gradients in the surface normal at the interface as

$$\boldsymbol{n}_l = \frac{\nabla C}{|\nabla C|}, \tag{7}$$

and the contact angle effects are considered by applying Young's law at the triple line region:

$$\boldsymbol{n} = \boldsymbol{n}_w \cos\theta \boldsymbol{\tau}_s + \sin\theta, \tag{8}$$

with $\boldsymbol{n}_w$ is the normal unit vector to the wall, $\boldsymbol{\tau}_s$ is the tangential unit vector toward the wetting phase and θ is the contact angle.

Generation of GDL surfaces

In practice, GDL materials have complex and heterogeneous nature, where the mean surface roughness height of commercial GDL ranges from 8 to 46 μm and RMS roughness (R_q) ranges from 10 to 45 μm for over 20 types of testing samples [47]. Therefore, it is of great significance to have a satisfactory representation of rough surfaces for simulating droplet dynamics on GDL. Various approaches have been proposed for rough surface modelling, including the random process such as Gaussian or exponential function [48] and fractal-based techniques like the Weierstrass–Mandelbrot fractal function [49]. In this work, the Gaussian height distribution function and autocovariance function are adopted to generate the targeted rough surfaces [50], and the roughness parameters are characterised by the RMS roughness (R_q) containing the vertical information and roughness wavelength (R_w) for the lateral information. The lateral position of surface point x is uniformly distributed on the surface with i_{th} surface point expressed as:

$$x_i = (i-1)\cdot\frac{L}{N-1}; i = 1, 2, 3, \ldots, N, \tag{9}$$

where N is the total number of points used for surface generation and L is the total length of the surface.

The height of the rough surface point Z follows the Gaussian distribution function:

$$p(Z) = \frac{h}{\sqrt{2\pi}} e^{-\frac{z^2}{2}}, \tag{10}$$

where p is cumulative probability, and the h is the standard deviation. Then convolution, inverse Fourier transform and normalising prefactors are subsequently used to correlate the surface:

$$Z = \sqrt{\frac{2}{\sqrt{\pi}}} \cdot \sqrt{\frac{Lc}{N}} \cdot f[\mathscr{F}[Z] \cdot \mathscr{F}[G]], \tag{11}$$

where c is the roughness wavelength (R_w), representing the typical distance between two similar features, e.g., valley or peaks of a surface, $\mathscr{F}$ and f are the forward and inverse transforms of Discrete Fourier Transform pair [51]:

$$\mathscr{F}[k] = \sum_{n=1}^{N} f[n] e^{-\frac{j2\pi(k-1)(n-1)}{N}}, (k = 1, 2, \cdots, N), \tag{12}$$

$$f[n] = \frac{1}{N}\sum_{k=1}^{N} \mathscr{F}[k] e^{\frac{j2\pi(k-1)(n-1)}{N}}, (n = 1, 2, \cdots, N), \tag{13}$$

and G is Gaussian filter based on the lateral location of surface points x:

$$G = e^{\left(-\frac{2x^2}{c^2}\right)}. \tag{14}$$

The morphology of the generated rough surface is controlled by two key parameters. One is the standard deviation h that determines the RMS roughness by altering the height distribution of generated data points, and the other is wavelength c which describes the distances between similar roughness features. In this study, the RMS roughness (R_q) is selected as 10, 20, 30 and 40 μm which are within the range of GDL surface roughness reported by El-Kharouf et al. [47], and R_q of each generated surface is recalculated to ensure the deviation to the target value is within 2%, where $R_q = \sqrt{\frac{1}{N}\sum_{i=1}^{N} Z_i^2}$. Though the value of R_w for GDL material is not mentioned in the literature, and in order to examine the effects of surface roughness lateral information on droplet dynamics, R_w is selected as 10, 20, 50 and 100 μm for simulations.

In GDL, R_w can be correlated to the carbon fibre arrangement, as shown in Fig. 1. Here, N is selected as 1500 to provide a high resolution of surface roughness. The samples of generated surfaces with different roughness parameters are shown in Fig. 2.

The height distribution of each generated surface is examined by the Gaussian fitting as well as the Quantile-Quantile (Q-Q) plot as shown in Fig. 3. The R-square of Gaussian fitting on generated surface is required to be larger than 0.9 for a qualified statistical representation, and the data points in the Q-Q plot should be inbound the interval based on 95% confidence level.

Computational domain and operational conditions

The computational domain of the flow channel with a rough substrate is shown in Fig. 4. The dimension of flow channel and operation parameters are determined based on various design and numerical studies [38,44,52–54]. The length and height of the geometry is 1.5 mm and 0.3 mm, respectively. The location of GDL pore is set at 0.2 mm right to the air inlet to ensure a stable airflow profile is developed before reaching the droplet, and the water injection pore size is 5 μm. The generated data points are connected into rough surface using AutoCAD software with all other boundaries being prescribed, and the section designed for droplet emergence is replaced by a water inlet channel. The geometry of computational domain is then imported into the FLUENT as an SAT file [56]. To describe the roughness features in the CFD domain, a refined mesh shown in Fig. 4 with element size of 1.5 μm has been generated at the rough surface layer to match point-by-point with the substrate boundary. The left wall is set as velocity-inlet boundary condition for airflow, and the right wall is a pressure-outlet boundary condition (with gauge pressure p = 0 kPa). The inlet velocity for airflow is chosen as 5, 15 and 25 m/s. The speed of 1 m/s is selected as the water inlet velocity based on the existing literature on the choice of water inlet velocity [36,52,55]. Although 1 m/s is beyond the water production rate of PEMFCs at high power density operation condition, this value is adapted for accelerating water accumulation rate due to the limitation of the computational resource. A practical actual water inlet speed can be implemented, but this will not significantly impact on the dependence of water removal efficiency on the GDL roughness, as discussed in the later sections. The intrinsic contact angle for GDL material typically ranges from 120° to 150° [15,16]. Therefore, the wettability of rough surface in this work is set to 140° to ensure the hydrophobicity of the bottom substrate, and the wettability of the top wall is set to 90°. No-slip

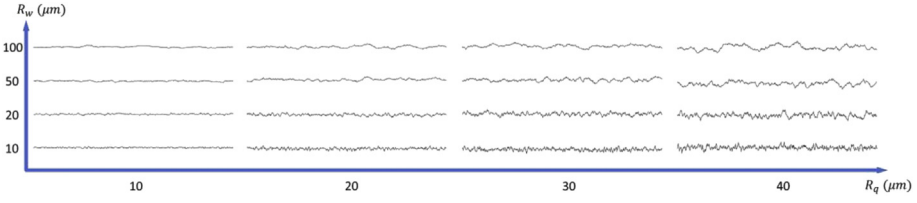

Fig. 2 – Typical samples of surfaces with various roughness parameters.

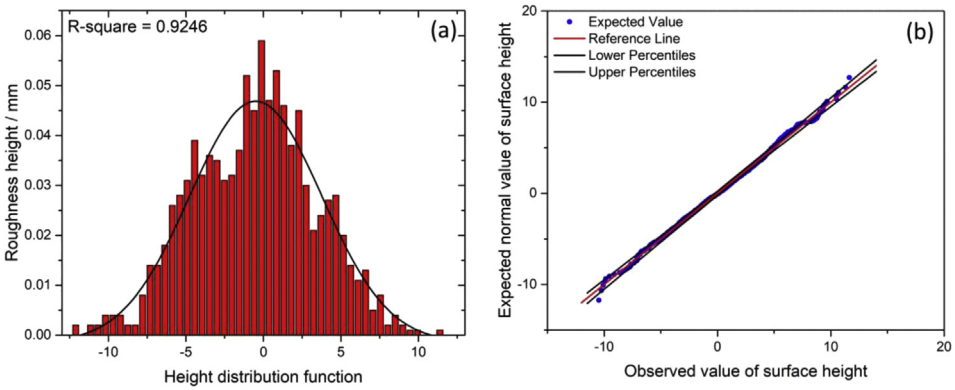

Fig. 3 – Generated surface profiles examined by (a) Histogram with Gaussian fitting, (b) Quantile-Quantile plot with 95% confidence level.

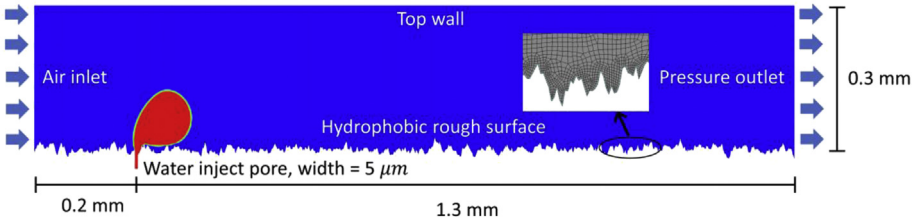

Fig. 4 – The computational domain of a flow channel with rough surface, with an insert showing a layer of refined mesh at the rough surface.

boundary condition is prescribed for both the top wall and rough substrate.

Numerical solutions

The airflow and liquid water in the simulation are assumed to be isothermal and incompressible with constant fluid properties. The governing equations are discretised by finite volume method, and the segregated pressure-based algorithm is selected for solving the Navier-Stokes and volume fraction equations. The momentum equation is solved by the quick differencing scheme for minimizing the numerical diffusion, and the transient formulation is solved by the bounded second order implicit scheme. The pressure and velocity scheme are coupled by the pressure-implicit with splitting of operators (i.e., PISO algorithm) to improve the convergence rate with high accuracy. The simulation is performed in ANSYS FLUENT®18.2 [56]. Mesh sensitivity analysis has been conducted with three different element sizes: 3.2, 2.7 and 2.2 μm, and 2.7 μm is selected for mesh due to the mesh convergence as shown in Fig. 5. Three different time steps 10^{-7}, 5×10^{-7} and 10^{-8} s are used for time step independence test. Through the sensitivity tests, 10^{-7} s is chosen for the simulation as no obvious difference in terms of the observed droplet dynamics is recorded if the time step is further reduced (e.g., 5×10^{-7} and 10^{-8} s). The maximal iterations per time step is 100, and 10^{-4} is selected as the converge criterion for all the variables. In addition, the repeatability and consistency of the emerging, growing, detachment and removal cycle of liquid droplet are examined on different surfaces. The droplet removal cycles are repeated for several times, and no obvious difference in detachment time or droplet shape for a given surface is observed in every single test as shown later in Fig. 6(b) (only three typical repetitions are presented out of over 10 simulated cycles). It's worth noting that multiple droplets can be present and removed at the same time in the flow channel during the operation of PEMFCs [40,45]. Multiple droplets can be either removed separately or merge into a single droplet then blown away by the airflow, which could influence the

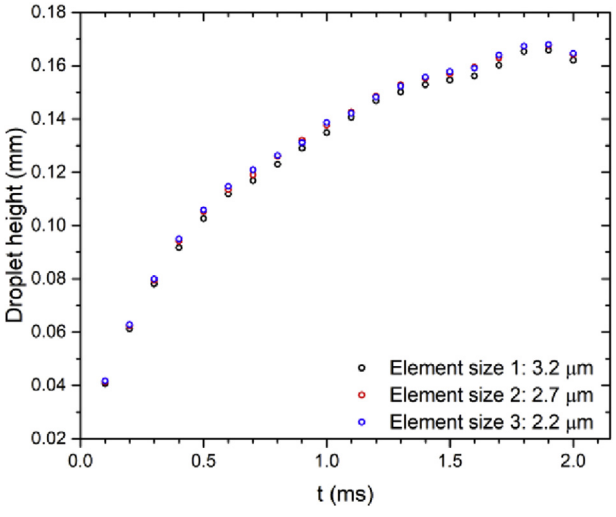

Fig. 5 – Grid independent test by recording droplet height during the emergence process.

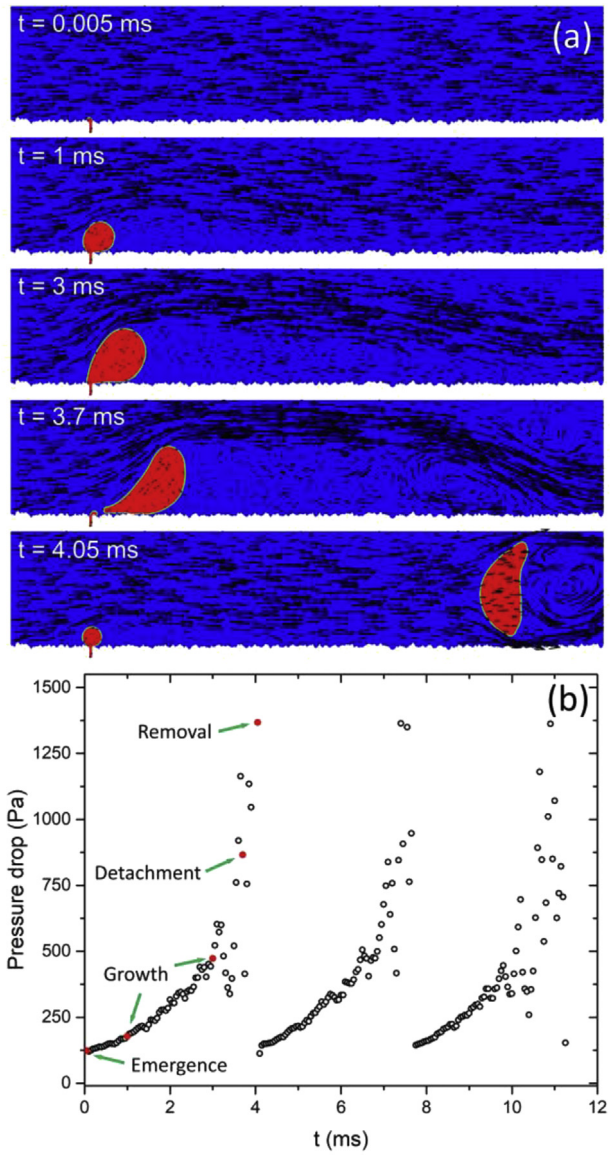

Fig. 6 – (a) Emergence, growth, detachment, and removal during droplet drainage process, and (b) Pressure drop measured in GDL flow channel with the red solid dots indicating the corresponding cases in (a). (For interpretation of the references to color in this figure legend, the reader is referred to the Web version of this article.)

droplet volume being removed and flow field conditions such as pressure drop and channel blockage. In this work, single droplet removal with different volume and flow field conditions are investigated in the following sections emphasising the effects of surface roughness, therefore multiple droplets removal scenarios are not incorporated in current study. The model has been validated by simulating droplet movement with fixed volume on both smooth and rough surface, and the results are qualitatively comparable to the results reported Refs. [38,52]. Therefore, the droplet dynamics is only simulated for the first emerged droplet in this work due to the repeatability demonstrated. Table 1 summarises the geometrical and material parameters used in the simulation.

Table 1 – Geometrical and material parameters.

Parameters	Symbols	Value
Channel height (mm)	h_c	0.3
Channel width (mm)	h_w	1.5
Pore size (μm)	w	5
Airflow rate (m/s)	v_a	5, 15, 25
Air density (kg/m^3)	ρ_a	1.225
Air viscosity (kg/m-s)	η_a	1.7894×10^{-5}
Water inlet velocity (m/s)	v_w	1
Water density (kg/m^3)	ρ_w	998.2
Water viscosity (kg/m-s)	η_w	0.001003
Water surface tension (N/m)	γ	0.00728
GDL contact angle (°)	θ	140
RMS roughness (μm)	R_q	10, 20, 30, 40
Roughness wavelength (μm)	R_w	10, 20, 50, 100
Time step (sec)	Δt	10^{-7}
Mesh element size (m)	–	2.7×10^{-6}

Results and discussion

The movement and geometrical shape of a droplet emerging from a GDL pore are mainly influenced by a combination of several forces: (1) pressure force that arising from the pressure drop at different sides of the droplet; (2) shear force resulted by the airflow passing above the droplet; (3) adhesive force which is related to the contact area between the droplet and rough surface; (4) surface tension force due to the pressure difference at the water and air surface; and (5) other forces such as inertia force, gravity force and viscous force. The relative importance of surface tension force to other forces can be characterised by dimensionless numbers: Capillary number (Ca), Bond number (Bo) and Weber number (*We*):

$$Ca = \frac{\eta v}{\gamma}, \tag{15}$$

$$Bo = \frac{\rho g w^2}{\gamma}, \tag{16}$$

$$We = \frac{\rho v^2 w}{\gamma}, \tag{17}$$

which compares the contribution from viscous, gravity and inertia forces, respectively, with the surface tension. With the GDL pore width w used as characteristic length, we have $Ca = 0.014$, $Bo = 6.8 \times 10^{-7}$, $We = 0.069$. The relatively small values of these dimensionless numbers suggest that the surface tension force is more significant than viscous, gravity and inertia forces. Since the water injection rate and surface wettability are fixed in this work, the airflow rate that determines the pressure force and shear force together with the surface roughness that influences the apparent wettability and the adhesive force at the liquid-solid interface will be mainly studied in the following. Humidity of reactant gas should be considered when evaluating the removal efficiency of droplets in GDL and flow channel due to the potentially resulted phase change phenomenon and change of surface tension could. Nevertheless, this study mainly focuses on the effects of airflow velocity and GDL roughness on droplet removal, the effects of reactant gas humidity will be considered in future investigations.

Droplet dynamics on rough surfaces

A typical liquid drainage process inside a GDL flow channel including droplet emerging, growing, detachment, and removal is demonstrated in Fig. 6(a). In the beginning, the airflow is fully developed inside the flow channel and liquid water is gradually injected from the emergence pore. Then the droplet starts to grow until the pressure force and shear force overcome the surface tension and adhesive force, and the droplet is detached from the emergence pore, as a result. After the detachment, the airflow drives the liquid droplet out of the channel and another droplet emerges from the GDL pore simultaneously. Pressure drop is an important indicator to evaluate the water removal performance in flow channel, and it is directly related to the flow resistance during the removal process. In this study, the pressure drop is measured as the pressure difference between the airflow inlet and pressure outlet, and the value is averaged along the inlet/outlet boundary. The corresponding pressure drop throughout the whole liquid removal process is shown in Fig. 6(b). It can be seen that pressure drop gradually increases as the liquid water accumulates at the GDL surface. The pressure drop reaches the largest value immediately after the detachment, because the rolling droplet blocks part of the flow channel during the removal process. Once the droplet is drained out of the channel, the pressure drop falls down and the similar process repeats for the next emerging droplet.

Airflow rate

Airflow rate should be carefully monitored during the operation of PEMFCs for maintaining a stable and reliable performance. At the cathode side, air/oxygen is feed into the flow channel through the GDL, and liquid water is produced at the catalyst layer. A sufficient supply of airflow is desired for PEMFCs to ensure a high current density output, and the effects of airflow on the droplet dynamics have been investigated in several studies [19–21,52,57]. In this section, the droplet detachment, elongation, and moving mechanism subject to various airflow rates on rough surfaces will be studied. Rough surfaces with R_q of 10, 20, 30 and 40 μm and $R_w$of 10 μm are applied to study the effects of airflow rate on droplet dynamics. Three realisations of rough surfaces with same roughness parameters are generated, and airflow rate with 5, 15 and 25 m/s are employed for simulations and analysis.

Droplet detachment time and elongation

The detachment time is referred to the time required for a droplet from emergence to detachment. For the constant injection rate, this is also directly associated with the maximum droplet size before the detachment. The droplet detachment time is critical for the evaluation of water removal efficiency as quick detachment of droplet leads to less water accumulation and faster flow drainage rate, and therefore facilitates water management inside the flow channel. Fig. 7(a) demonstrates the liquid droplet detachment time with three different airflow velocities, i.e., 5, 15 and 25 m/s on rough substrate. It's observed that a higher airflow rate significantly decreases detachment time of emerging droplet on same surface. Compared with airflow rate of 25 m/s, the detachment time is about doubled for the counterparts with 15 m/s and tripled for counterparts with 5 m/s. Moreover, the effects of surface roughness on the detachment time can also be clearly observed and will be discussed with more details in GDL roughness

The droplet elongation is another important parameter for assessing the water management efficiency, which describes the droplet contact area on the rough surface before the detachment. The elongated droplet blocks the pathway for air and water passing through the gas diffusion material, therefore this blockage should be minimized during the water drainage process. Fig. 7 (b) shows the effect of airflow rate on the droplet elongation and the results suggest that the droplet elongation is significantly reduced by increasing the airflow rate. This trend is similar to the effects on droplet detachment time because a larger droplet contact area can be typically observed with higher droplet volume.

The effects of airflow rate on droplet detachment and elongation reduction are mainly attributed to the pressure drop resulted from different flow rates. The pressure drop throughout the liquid removal process on a given surface subject to different airflow rates are demonstrated in Fig. 8. It can be seen that a higher airflow rate leads to a quicker change in the pressure drop, i.e., a larger sudden change of inlet pressure at the moment of detachment, while the pressure drop values required for the detachment are similar. Therefore, the time required for reaching the critical detachment pressure drop is less for the case with higher airflow rate, in which the droplet is blown away at earlier stage.

Modes of droplet motion

The motion and shape of the detached droplets are greatly influenced by airflow rate. Fig. 9 shows three typical droplet movement modes (rolling, lifting, and breakup) after the detachment. In the rolling mode, the droplet demonstrates a transitional behaviour on the rough substrate. The lifting mode refers to the droplet is lifted in the channel after its detachment, and the droplet may touch the top substrate before its drained out. For the breakup mode, the droplet firstly rolls on rough surface after the detachment and then breaks up on the substrate. The occurrence of three different moving modes is mainly influenced by the airflow rate as shown in Fig. 10, and no obvious effects of surface roughness on droplet movement modes are observed. For airflow rate with 5 and 15 m/s, rolling mode has more occurrences, and for 25 m/s the breakup mode dominates. The breakup mode is not favourable for the water management as some of the separated droplets keep adhering to the rough surface as shown in Fig. 9. These small droplets staying in the valleys of rough surface are very difficult to be removed from the channel, and these droplets block the pathway for air and water transport through the gas diffusion media. For the rolling mode, the detached droplet is in contact with the GDL surface during the removal process, however, this blockage is almost negligible considering the relatively short period of time of removal process and therefore makes the rolling mode favourable. Lifting is the optimal mode to facilitate the water removal efficiency since the gas diffusion media keeps uncovered and drained after the detachment, and the droplet can be easily removed even it is temporally adhered to the top wall.

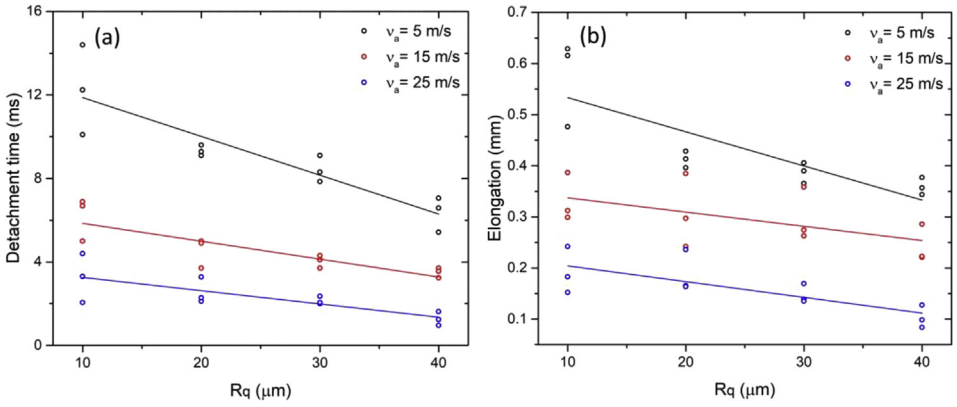

Fig. 7 – The effects of airflow rate on droplet (a) detachment time and (b) elongation.

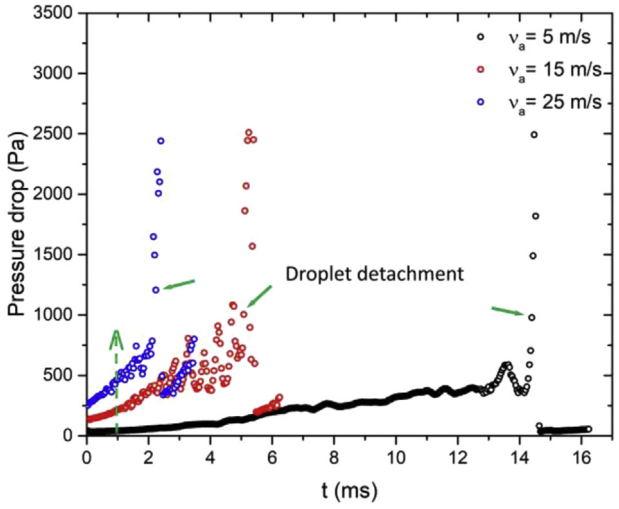

Fig. 8 – The effects of airflow rate on the pressure drop.

Based on the above analysis on the detachment time, elongation and movement modes, 15 m/s is considered as the optimal operational parameter for airflow rate in water management, as 5 m/s leads to a relatively larger droplet detachment time and elongation, and 25 m/s could result in water accumulation and blockage in flow channel due to the separated droplets remaining on the GDL surface.

GDL roughness

In this section, the effects of GDL surface roughness on water management are examined. The RMS roughness (R_q) is selected as 10, 20, 30, 40 μm with roughness wavelength $(R_w)$of 10, 20, 50, 100 μm, and airflow rate is fixed as 15 m/s. In total of 16 combinations of surface parameters are employed, and for each combination, 10 random samples of surface geometries are generated to provide statistical analysis. Thus, a total of 160 simulations are conducted and analysed.

Droplet breakup position and detachment ratio

The breakup position (x_b) is the horizontal location where the droplet is detached from the emergence pore. x_b ranges from 0.2 mm to 1.5 mm except for the cases with no detached droplet, i.e., $x_b \geq 1.5mm$. The detachment ratio (α) is defined as the ratio between volume of detached droplet V_d and total liquid volume emerged V_t as $\alpha = \frac{V_d}{V_t}$. Three regimes of droplet detachment are identified according to the different breakup positions and detachment ratios, and Fig. 11 demonstrates samples of droplet morphology in each regime and breakup positions for all simulations. In Regime 1, x_b is smaller than 0.4 mm and the detachment ratio is above 95%. For Regime 2, x_b is between 0.4 mm and 1.5 mm, and detachment ratio is below 95%. In Regime 3, the droplet is not detached and a liquid film is formed on the substrate even after the liquid front reaches the pressure outlet.

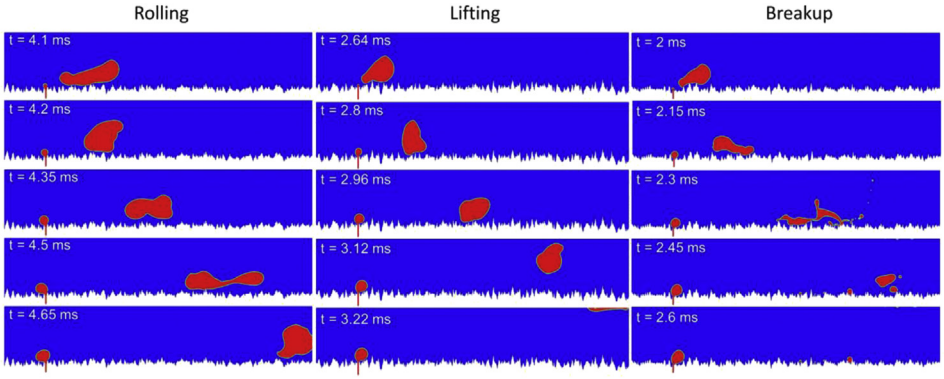

Fig. 9 – Evolutions of droplet morphology under different movement modes.

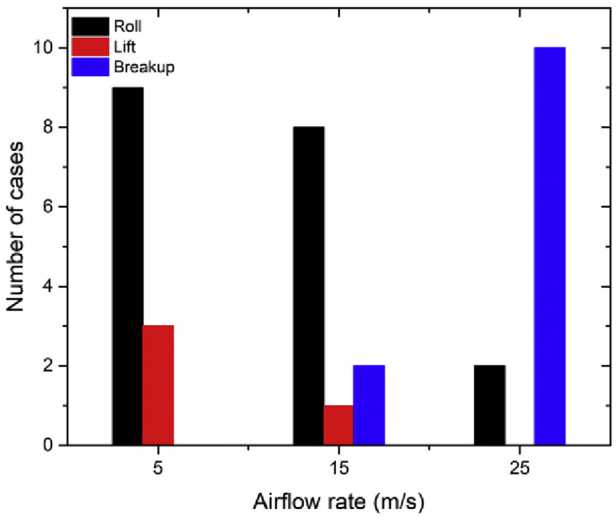

Fig. 10 – Number of cases for different movement modes.

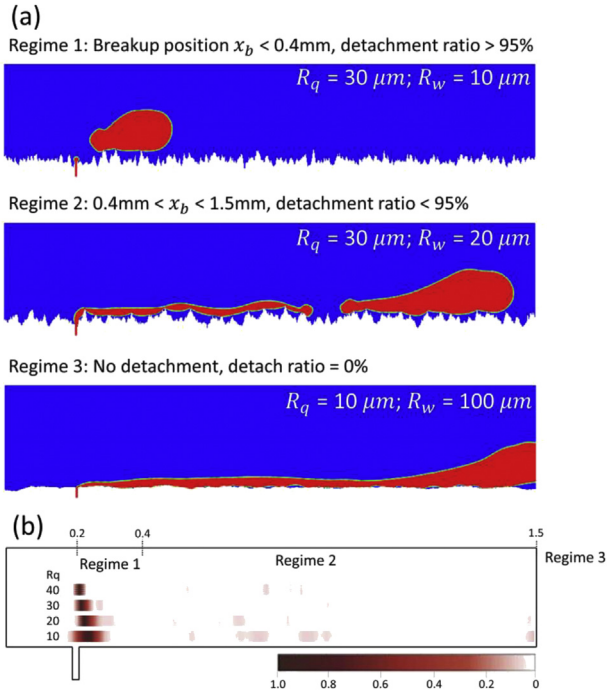

Fig. 11 – (a) Droplet morphology for three different detachment regimes and (b) Smoothed probability density histogram of droplet detachment position for all simulations (from 40 cases for each RMS roughness).

Fig. 12(a) summarises the number of cases in each regime on different rough surfaces, at the given operational condition. There are in total 40 cases for each R_q value, which includes samples with all 4 different R_w scenarios. It can be seen that Regime 1 accounts for the majority of the cases for all surfaces with different roughness parameters, and Regime 2 has much fewer occurrences compared with Regime 1. Regime 3 only happens on smoother surfaces with R_q of 10 and 20 μm. This result can be attributed to the different wetting types when a droplet contacts with the solid rough substrate. The first type is Wenzel state where the droplet fills the gaps between the heterogeneous microstructures and a complete wetting is observed [58]. Cassie state is another wetting type which refers to the droplet resting on top of surface and leaving air trapped in the gap beneath the droplet [59]. Experimental observations have reported the coexistence of Cassie and Wenzel state on GDL surface [60]. Fig. 12(b) presented two simulation snapshots for droplets growing on different rough GDL surfaces demonstrating Cassie and Wenzel states, respectively. It is found that the emerged droplets in Regime 1 and 2 are mostly in Cassie state, and the contact area between the rough surface and droplet is significantly small compared to the projection area. Therefore, the adhesive force is greatly reduced at the solid-liquid interface, and the pressure force overcomes the resistance force easily and blows the droplet out of the flow channel. A typical example existing in nature to illustrate the droplet removal behaviour with Cassie state is lotus leaves, where droplets resting on super-hydrophobic surfaces with micro-patterns are easily to be removed [61]. For Regime 3, the simulation results suggested that Wenzel state dominates the wetting type. The contact area at the interface and resulted adhesive force keep increasing with the formation and elongation of water film, and the pressure force can only stretch the droplet instead of breaking up the droplet. Regime 1 is the favourable detachment mode for water management because of the relatively higher detachment ratio, and the breakup position is near the GDL pore leading to less blockage of GDL surface as a result. Regime 2 is less favourable for water removal as part of GDL surface is covered by the droplet before the detachment, and the detachment ratio is smaller than Regime 1. In Regime 3, the formed water film completely blocks the pathway for both air and water, and no detachment occurs even after the droplet reaches the end of flow channel. Though the probability of having Regime 3 is low, this could result in serious performance degradation and it should be avoided during the operation of PEMFCs.

Detachment time and elongation

The effects of GDL surface roughness on droplet detachment time and elongation in Regime 1 are investigated, since Regime 1 is the most preferable detachment mode and accounts for the majority of simulated cases. Fig. 13 presents the effects of RMS roughness on droplet detachment time and elongation. It is demonstrated that both detachment time and elongation decrease with the increase of R_q for all surfaces with various roughness wavelength. The Pearson's correlation coefficient r is employed to evaluate the linear correlation between the variables and R_q [62]. The value of Pearson's r between 0 and 0.3 (0 and −0.3) suggests a weak positive (negative) linear relationship. Value between 0.3 and 0.7 (−0.3 and −0.7) refers to a relatively strong positive (negative) linear relationship. Value between 0.7 and 1.0 (−0.7 and −1.0) indicates a strong positive (negative) linear relationship [63]. In terms of the correlation between detachment time and R_q, the Pearson's r is −0.70 for simulations conducted with R_w of 10 μm, which indicates a strong correlation, and for the cases with R_w of 20, 50 and 100 μm, relatively strong correlations are suggested with −0.50, −0.55 and −0.63 for Pearson's r. For droplet elongation, all simulations

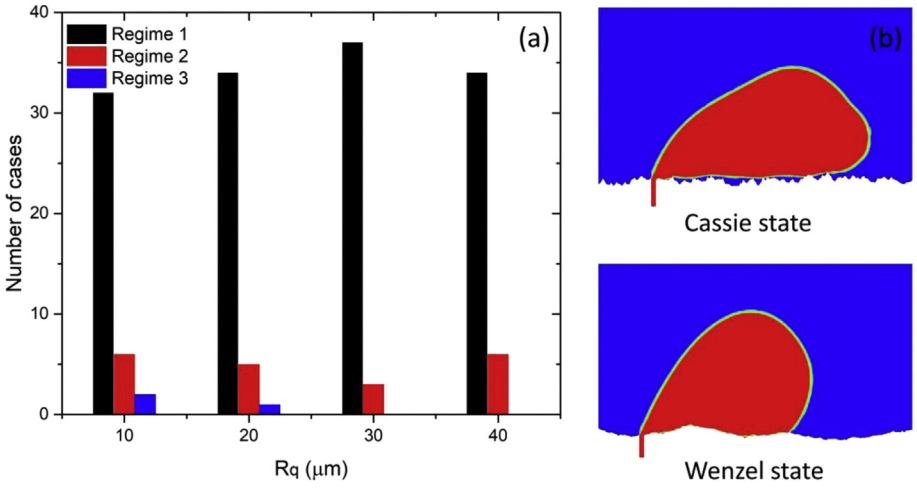

Fig. 12 – (a) Number of cases in each regime; (b) Typical Cassie and Wenzel state for an emerged droplet on rough GDL surfaces.

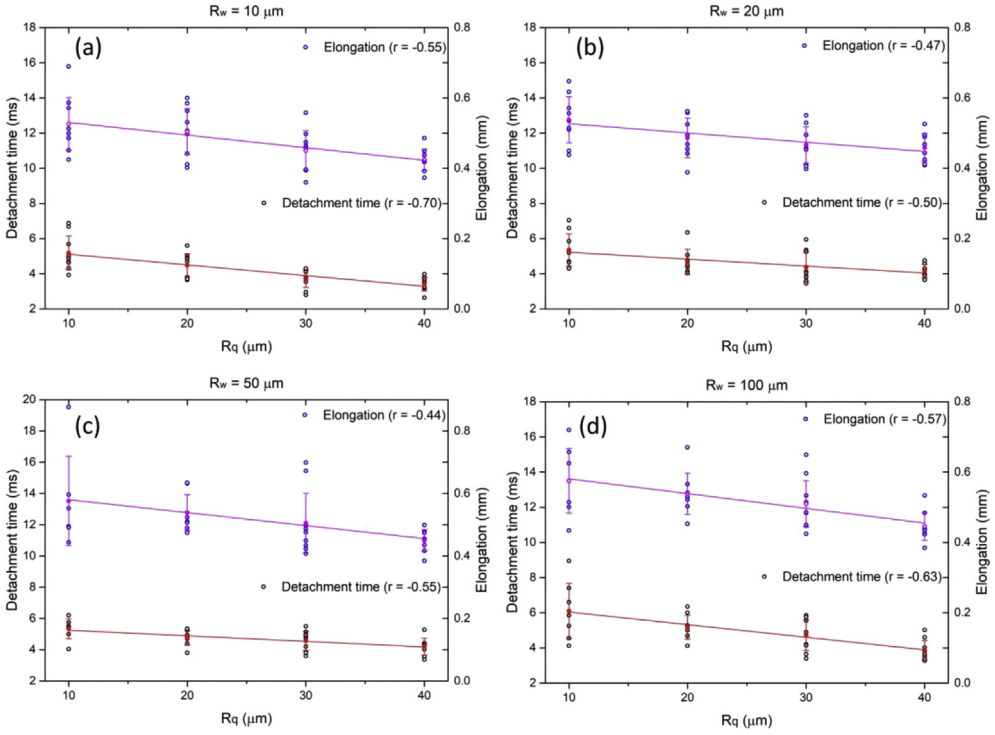

Fig. 13 – Effects of R_q on droplet detachment time and elongation with R_w fixed to (a) 10, (b) 20, (c) 50, and (d) 100 μm respectively.

reported a relatively strong correlation between elongation and R_q, which is similar to the results for detachment time. The average reduction of detachment time and elongation is about 30% and 20%, respectively, when R_q is increased from 10 μm to 40 μm based on all simulation cases. Therefore, the simulation results suggest that increasing the surface RMS roughness can accelerate detachment of droplet and mitigate the surface blockage on GDL material. This conclusion is in accordance with experimental observations, where Fishman et al. (2010) reported that GDL surfaces with smaller average roughness demonstrate a stronger pinning effect compared with ones with rougher surfaces, indicating that rough surface is favourable for the droplet detachment [64]. In addition, the results demonstrated the benefits of increasing RMS roughness on liquid removal, which is supplementary to numerical findings conducted on patterned surfaces by He et al. (2010) and Chen et al. (2013) [34,37]. The results can be compared with 3D numerical solutions to verify the effects of surface roughness on droplet removal in GDL channels. Chen et al. (2012) constructed rough GDL surface with cubic

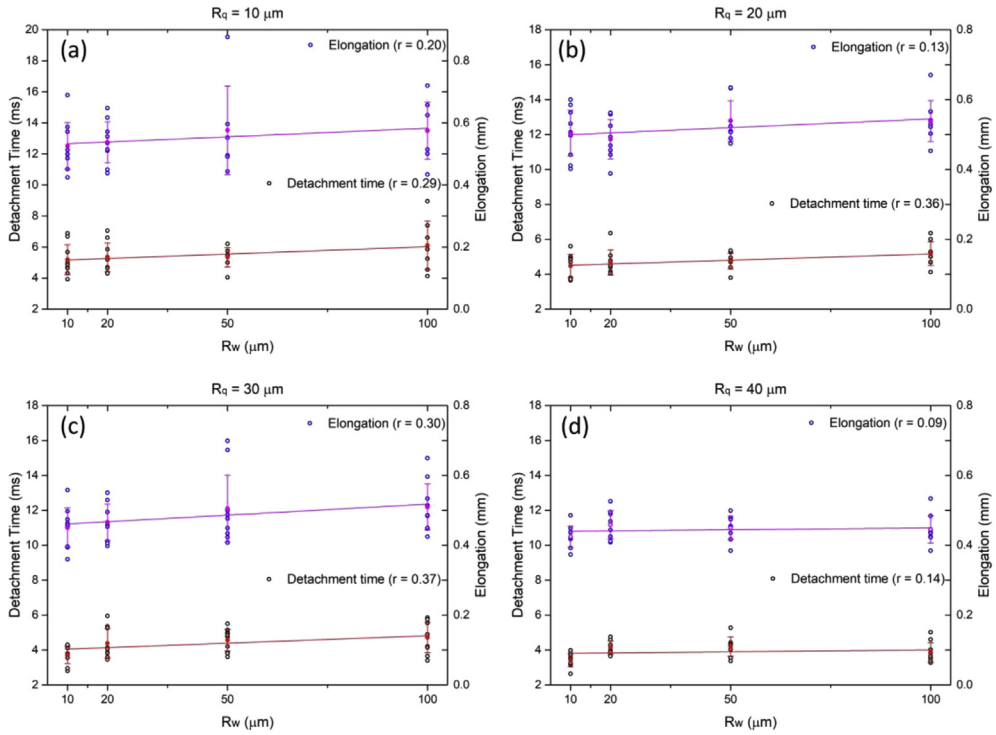

Fig. 14 – Effects of R_w on droplet detachment time and elongation with R_q fixed to (a) 10, (b) 20, (c) 30, (4) 40 μm respectively.

columns, in which the spacing and height of columns are altered to represent surfaces with different roughness [36]. They concluded that increasing surface roughness assists the removal of emerging droplet in terms of shorter removal time, which is in accordance with our findings as discussed above.

The results report a relatively large standard deviation of data for surfaces with same roughness parameters, and this can be attributed to the heterogeneity of the generated GDL surface profile and geometry. Since all the simulations taken into consideration is in Regime 1, the different surface geometry near the GDL pore region has significantly influenced the droplet detachment and elongation even with same roughness parameters. Although the standard deviation is relatively large, a clear correlation is identified to prove the effects of RMS roughness on droplet detachment.

Moreover, the effects of R_w on droplet detachment time and elongation are presented in Fig. 14. The results suggest that the R_w has a weak positive linear relationship with both droplet detachment time and elongation as none of the Pearson's r values is above 0.4. This conclusion indicates that roughness wavelength is less significant to water removal efficiency compared with RMS roughness.

Conclusion

In this study, the effects of airflow rate and GDL surface roughness on the droplet detachment and removal efficiency are investigated using the VOF method. The rough surfaces are characterised by RMS roughness (R_q) and roughness wavelength (R_w) containing both lateral and vertical roughness information, and the dynamics of droplet from emergence to removal are fully incorporated. Rolling, lifting, and breakup are identified as three different droplet movement modes on rough surface subject to various airflow rates, and numerical solution suggests an optimal airflow rate best facilitating the water management inside GDL channel for the given channel geometry. Moreover, the water removal is further examined on surfaces with various roughness parameters, and different regimes for water removal are classified based on detachment ratio and droplet breakup location. The results demonstrate the existence of two wetting types, where rougher surfaces usually resulting in Cassie state are favourable for the liquid detachment because less water film and surface blockage are observed on such surfaces. Furthermore, increasing RMS roughness can significantly improve water drainage efficiency by reducing the droplet detachment time and elongation, while the effects of roughness wavelength on liquid removal are less influential. Our study highlights the importance of GDL surface roughness on the effective water management in fuel cells, and warrants future studies incorporating such morphological effects in the GDL design.

Acknowledgements

This work was financially supported by Australian Research Council (Projects DP170102886) and The University of Sydney SOAR Fellowship. This research was undertaken with the assistance of the HPC service at The University of Sydney.

REFERENCES

[1] Hau E. Wind turbines: fundamentals, technologies, application, economics. Springer Science & Business Media; 2013.
[2] Armstrong S, Hurley WG. A thermal model for photovoltaic panels under varying atmospheric conditions. Appl Therm Eng 2010;30(11–12):1488–95.
[3] Close DJ. The performance of solar water heaters with natural circulation. Sol Energy 1962;6:33–40.
[4] Acar C, Dincer I. The potential role of hydrogen as a sustainable transportation fuel to combat global warming. Int J Hydrogen Energy 2020;45(5):3396–406.
[5] Cipriani G, Di Dio V, Genduso F, La Cascia D, Liga R, Miceli R, et al. Perspective on hydrogen energy Carrier and its automotive applications. Int J Hydrogen Energy 2014;39(16):8482–94.
[6] Wang L, Husar A, Zhou T, Liu H. A parametric study of PEM fuel cell performances. Int J Hydrogen Energy 2003;28:1263–72.
[7] Rabbani A, Rokni M, Hosseinzadeh E, Mortensen HH. The start-up analysis of a PEM fuel cell system in vehicles. Int J Green Energy 2014;11:91–111.
[8] Jiao K, Li X. Water transport in polymer electrolyte membrane fuel cells. Prog Energy Combust Sci 2011;37:221–91.
[9] Cho JIS, Neville TP, Trogadas P, Bailey J, Shearing P, Brett DJL, Coppens MO. Capillaries for water management in polymer electrolyte membrane fuel cells. Int J Hydrogen Energy 2018;43(48):21949–58.
[10] Owejan JP, Gagliardo JJ, Sergi JM, Kandlikar SG, Trabold TA. Water management studies in PEM fuel cells, Part I: fuel cell design and in situ water distributions. Int J Hydrogen Energy 2009;34:3436–44.
[11] Lu Z, Kandlikar SG, Rath C, Grimm M, Domigan W, White AD, et al. Water management studies in PEM fuel cells, Part II: ex situ investigation of flow maldistribution, pressure drop and two-phase flow pattern in gas channels. Int J Hydrogen Energy 2009;34(8):3445–56.
[12] Andersson M, Beale SB, Espinoza M, Wu Z, Lehnert W. A review of cell-scale multiphase flow modeling, including water management, in polymer electrolyte fuel cells. Appl Energy 2016;180:757–78.
[13] Park GG, Sohn YJ, Yang TH, Yoon YG, Lee WY, Kim CS. Effect of PTFE contents in the gas diffusion media on the performance of PEMFC. J Power Sources 2004;131:182–7.
[14] Omrani R, Shabani B. Gas diffusion layer modifications and treatments for improving the performance of proton exchange membrane fuel cells and electrolysers: a review. Int J Hydrogen Energy 2017;42:28515–36.
[15] Mortazavi M, Tajiri K. Effect of the PTFE content in the gas diffusion layer on water transport in polymer electrolyte fuel cells (PEFCs). J Power Sources 2014;245:236–44.
[16] Lim C, Wang CY. Effects of hydrophobic polymer content in GDL on power performance of a PEM fuel cell. Electrochim Acta 2004;49:4149–56.
[17] Utaka Y, Koresawa R. Performance enhancement of polymer electrolyte fuel cells by combining liquid removal mechanisms of a gas diffusion layer with wettability distribution and a gas channel with microgrooves. J Power Sources 2016;323:37–43.
[18] Forner-Cuenca A, Biesdorf J, Gubler L, Kristiansen PM, Schmidt TJ, Boillat P. Engineered water highways in fuel cells: radiation grafting of gas diffusion layers. Adv Mater 2015;27:6317–22.
[19] Zhang FY, Yang XG, Wang CY. Liquid water removal from a polymer electrolyte fuel cell. J Electrochem Soc 2006;153:225–32.
[20] Suresh PV, Jayanti S. Effect of air flow on liquid water transport through a hydrophobic gas diffusion layer of a polymer electrolyte membrane fuel cell. Int J Hydrogen Energy 2010;35:6872–86.
[21] Chen R, Qin Y, Ma S, Du Q. Numerical simulation of liquid water emerging and transport in the flow channel of PEMFC using the volume of fluid method. Int J Hydrogen Energy 2020. in press.
[22] Liu X, Guo H, Ma C. Water flooding and two-phase flow in cathode channels of proton exchange membrane fuel cells. J Power Sources 2006;156:267–80.
[23] Ous T, Arcoumanis C. Visualisation of water accumulation in the flow channels of PEMFC under various operating conditions. J Power Sources 2009;187:182–9.
[24] Ijaodola OS, El-Hassan Z, Ogungbemi E, Khatib FN, Wilberforce T, Thompson J, Olabi AG. Energy efficiency improvements by investigating the water flooding management on proton exchange membrane fuel cell (PEMFC). Energy 2019;179:246–67.
[25] Zhang Z, Jia L, Wang X, Ba L. Effects of inlet humidification on PEM fuel cell dynamic behaviors. Int J Energy Res 2011;35:376–88.
[26] Guo N, Leu MC, Koylu UO. Network based optimization model for pin-type flow field of polymer electrolyte membrane fuel cell. Int J Hydrogen Energy 2013;38:6750–61.
[27] Reiser CA, Sawyer RD, inventors; Utc Power LLC, assignee. Solid polymer electrolyte fuel cell stack water management system. US Patent 1988; 4,769,297.
[28] Pellegri A, Spaziante PM. Bipolar separator for electrochemical cells and method of preparation thereof. US Patent 1980; 4,197,178.
[29] Voss HH, Chow C.Y. Coolant flow field plate for electrochemical fuel cells. US Patent 1993; 5,230,966.
[30] Spurrier FR, Pierce BL, Wright MK Fuel cell plates with improved arrangement of process channels for enhanced pressure drop across the plates. US Patent 1986; 4,631,239.
[31] Guo N, Leu MC, Koylu UO. Optimization of parallel and serpentine configurations for polymer electrolyte membrane fuel cells. Fuel Cell 2014;14(6):876–85.
[32] Chow CY, Wozniczka B, Chan JK Integrated reactant and coolant fluid flow field layer for an electrochemical fuel cell. US Patent 1998; 5,804,326.
[33] Wood D. Collapse and fragmentation of isothermal gas clouds. Royal Astronomical Society 1981;194:201–18.
[34] He G, Yamazaki Y, Abudula A. The effect of wall roughness on the liquid removal in micro-channels related to a proton exchange membrane fuel cell (PEMFC). J Power Sources 2010;195:1561–8.
[35] Ding Y, Bi HT, Wilkinson DP. Three-dimensional numerical simulation of water droplet emerging from a gas diffusion layer surface in micro-channels. J Power Sources 2010;195:7278–88.
[36] Chen L, Luan H, He YL, Tao WQ. Effects of roughness of gas diffusion layer surface on liquid water transport in micro gas channels of a proton exchange membrane fuel cell. Numer Heat Tr A-Appl 2012;62:295–318.
[37] Chen L, He YL, Tao WQ. Effects of surface microstructures of gas diffusion layer on water droplet dynamic behaviors in a micro gas channel of proton exchange membrane fuel cells. Int J Heat Mass Tran 2013;60:252–62.
[38] Ashrafi M, Shams M. Effects of heterogeneous surface of gas diffusion layers on droplet transport in microchannels of PEM fuel cells. Int J Hydrogen Energy 2016;41:1974–89.
[39] Zhan Z, Wang C, Fu W, Pan M. Visualization of water transport in a transparent PEMFC. Int J Hydrogen Energy 2012;37:1094–105.
[40] Santamaria AD, Das PK, MacDonald JC, Weber AZ. Liquid-water interactions with gas-diffusion-layer surfaces. J Electrochem Soc 2014;161:1184–93.

[41] Theodorakakos A, Ous T, Gavaises M, Nouri JM, Nikolopoulos N, Yanagihara H. Dynamics of water droplets detached from porous surfaces of relevance to PEM fuel cells. J Colloid Interface Sci 2006;300:673–87.
[42] Carton JG, Lawlor V, Olabi AG, Hochenauer C, Zauner G. Water droplet accumulation and motion in PEM (Proton Exchange Membrane) fuel cell mini-channels. Energy 2012;39:63–73.
[43] Gao Y, Zhang X, Rama P, Chen R, Ostadi H, Jiang K. Lattice Boltzmann simulation of water and gas flow in porous gas diffusion layers in fuel cells reconstructed from micro-tomography. Comput Math Appl 2013;65:891–900.
[44] Kim KN, Kang JH, Lee SG, Nam JH, Kim CJ. Lattice Boltzmann simulation of liquid water transport in microporous and gas diffusion layers of polymer electrolyte membrane fuel cells. J Power Sources 2015;278:703–17.
[45] Xu Y, Peng L, Yi P, Lai X. Numerical investigation of liquid water dynamics in wave-like gas channels of PEMFCs. Int J Energy Res 2019;43(3):1191–202.
[46] Ju Brackbill, Kothe DB, Zemach C. A continuum method for modeling surface tension. J Comput Phys 1992;100:335–54.
[47] El-Kharouf A, Mason TJ, Brett DJ, Pollet BG. Ex-situ characterisation of gas diffusion layers for proton exchange membrane fuel cells. J Power Sources 2012;218:393–404.
[48] Ogilvy JA, Foster JR. Rough surfaces: Gaussian or exponential statistics? J Phys D Appl Phys 1989;22:1243.
[49] Berry MV, Lewis ZV, Nye JF. On the Weierstrass-Mandelbrot fractal function. Proc R Soc Lond A Math Phys Sci 1980;370:459–84.
[50] Garcia N, Stoll E. Monte Carlo calculation for electromagnetic-wave scattering from random rough surfaces. Phys Rev Lett 1984;52:1798.
[51] Frigo M, Johnson SG. The design and implementation of FFTW3. Proc IEEE 2005;93:216–31.
[52] Zhu X, Sui PC, Djilali N. Dynamic behaviour of liquid water emerging from a GDL pore into a PEMFC gas flow channel. J Power Sources 2007;172:287–95.
[53] Han B, Yu J, Meng H. Lattice Boltzmann simulations of liquid droplets development and interaction in a gas channel of a proton exchange membrane fuel cell. J Power Sources 2012;202:175–83.
[54] Hossain M, Islam SZ, Colley-Davies A, Adom E. Water dynamics inside a cathode channel of a polymer electrolyte membrane fuel cell. Renew Energy 2013;50:763–79.
[55] Cai Y, Yang T, Sui PC, Xiao J. A numerical investigation on the effects of water inlet location and channel surface properties on water transport in PEMFC cathode channels. Int J Hydrogen Energy 2016;41(36):16220–9.
[56] Guide. Release 18.2. A.F.U.s. Ansys Inc 2017.
[57] Wu TC, Djilali N. Experimental investigation of water droplet emergence in a model polymer electrolyte membrane fuel cell microchannel. J Power Sources 2012;208:248–56.
[58] Wenzel RN. Resistance of solid surfaces to wetting by water. Ind Eng Chem 1936;28:988–94.
[59] Cassie AB, Baxter S. Wettability of porous surfaces. Phys Chem Chem Phys 1944;40:546–51.
[60] Parry V, Berthomé G, Joud JC. Wetting properties of gas diffusion layers: application of the Cassie–Baxter and Wenzel equations. Appl Surf Sci 2012;258:5619–27.
[61] Koch K, Bhushan B, Barthlott W. Multifunctional surface structures of plants: an inspiration for biomimetics. Prog Mater Sci 2009;54(2):137–78.
[62] McGraw KO, Wong SP. Forming inferences about some intraclass correlation coefficients. Psychol Methods 1996;1:30.
[63] Ratner B. The correlation coefficient: its values range between+ 1/− 1, or do they? J Target Meas Anal Market 2009;17:139–42.
[64] Fishman JZ, Leung H, Bazylak A. Droplet pinning by PEM fuel cell GDL surfaces. Int J Hydrogen Energy 2010;35:9144–50.